ADVANCES IN ATMOSPHERIC SCIENCES, VOL. 36, JUNE 2019, 658–668

• **Original Paper** •

Indian Ocean Dipole–related Predictability Barriers Induced by Initial Errors in the Tropical Indian Ocean in a CGCM

Rong FENG[1] and Wansuo DUAN*[1,2]

[1]*State Key Laboratory of Numerical Modeling for Atmospheric Sciences and Geophysical Fluid Dynamics, Institute of Atmospheric Physics, Chinese Academy of Sciences, Beijing* 100029*, China*

[2]*University of Chinese Academy of Sciences, Beijing* 100049*, China*

(Received 17 October 2018; revised 30 January 2019; accepted 25 February 2019)

ABSTRACT

Using GFDL CM2p1 (Geophysical Fluid Dynamics Laboratory Climate Model, version 2p1), the effects of initial sea temperature errors on the predictability of the Indian Ocean Dipole (IOD) are explored. When initial temperature errors are superimposed on the tropical Indian Ocean, a winter predictability barrier (WPB) and a summer predictability barrier (SPB) exist in IOD predictions. The existence of the WPB has a close relation with El Niño–Southern Oscillation (ENSO) in the winter of the growing phase of positive IOD events. That is, when ENSO exists in winter, no WPB appears in IOD predictions, and vice versa. In contrast, there is no inherent connection between the existence of the SPB and ENSO. Only the dominant spatial pattern of SPB-related initial errors is studied in this paper, which presents a significant west–east dipole pattern in the tropical Indian Ocean and is similar to that of WPB-related initial errors in previous studies. The SPB-related initial errors superimposed on the tropical Indian Ocean induce the sea surface temperature (SST) and wind anomalies in the tropical Pacific Ocean. Then, under the interaction between the Indian and Pacific oceans through the atmospheric bridge and Indonesian Throughflow, a west–east dipole pattern of SST errors appears in summer, which is further strengthened under the Bjerknes feedback and yields a significant SPB.

Key words: predictability barrier, initial errors, Indian Ocean Dipole, Indian Ocean

Citation: Feng, R., and W. S. Duan, 2019: Indian Ocean Dipole–related predictability barriers induced by initial errors in the tropical Indian Ocean in a CGCM. *Adv. Atmos. Sci.*, **36**(6), 658–668, https://doi.org/10.1007/s00376-019-8224-9.

Article Highlights:

- When initial temperature errors are superimposed on the tropical Indian Ocean, a WPB and an SPB exist in IOD predictions.
- The existence of the WPB has a close relation with ENSO. There is no inherent connection between the existence of the SPB and ENSO.
- The dominant spatial pattern of SPB-related initial errors presents a significant west–east dipole pattern in the tropical Indian Ocean.

1. Introduction

As the dominant ocean–atmosphere coupled phenomenon of the interannual time scale in the tropical Indian Ocean, the Indian Ocean Dipole (IOD) has attracted considerable attention since the 1990s (Saji et al., 1999; Webster et al., 1999; Murtugudde et al., 2000). The IOD has positive and negative phases. The positive phase shows positive sea surface temperature anomalies (SSTAs) in the western Indian Ocean and negative SSTAs in the eastern Indian Ocean, accompanied by easterly wind anomalies at the equator. In contrast, the negative phase of the IOD features SSTA and wind anomaly patterns that are opposite to the positive phase. The intensity of IOD events is described by the dipole mode index (DMI), which is defined as the difference in SSTAs between the western Indian Ocean and eastern Indian Ocean (Saji et al., 1999). Positive IOD events usually induce high land surface temperatures and plentiful precipitation in East Africa, and vice versa in Indonesia and Australia (Ansell et al., 2000; Zubair et al., 2003; Behera et al., 2005). Besides, it could also modulate the climate in Europe, North America, South America, and Northeast Asia, via the propagation of planetary waves (Saji and Yamagata, 2003). Therefore, it is meaningful and urgent to study the predictability of IOD events and improve their forecast skill.

Previous studies have analyzed the forecast skill of IOD events in different models and shown that the lead time for

* Corresponding author: Wansuo DUAN
Email: duanws@lasg.iap.ac.cn

skillful predictions of IOD events is about one season, or sometimes two seasons for stronger ones (Wajsowicz, 2004, 2005; Luo et al., 2005, 2007; Shi et al., 2012). On the one hand, models are imperfect, and some cannot even simulate the basic characteristics of IOD events (Gualdi et al., 2003; Yamagata et al., 2004; Cai et al., 2005). That is, there are model errors in IOD predictions. On the other hand, errors in the initial field due to sparse observations is also a major limitation to the forecast skill (Luo et al., 2007; Feng and Duan, 2018). Feng et al. (2014a) demonstrated that a winter predictability barrier (WPB) exists in IOD predictions, which is caused by the initial errors in the tropical Indian Ocean. The WPB indicates that, whatever the start month, the forecast skill of IOD events decreases rapidly across winter (Luo et al., 2007). As IOD events usually reverse the sign of the DMI and occur in winter (Wajsowicz, 2004; Fig. 1), the existence of the WPB probably causes the low forecast skill of the occurrence of an IOD event. Furthermore, Liu et al. (2018) showed that, in addition to the WPB, there is also a significant summer predictability barrier (SPB) for IOD events, which is closely related with the initial errors in the tropical Pacific Ocean. The SPB indicates that, whatever the start month, the forecast skill decreases rapidly across the summer. As the DMI usually develops rapidly in summer (Wajsowicz, 2004; Fig. 1), the SPB greatly limits the forecast skill for the development of IOD events, and probably causes the low forecast skill of the IOD intensity

It has been demonstrated that only one third of IOD events are independent of El Niño–Southern Oscillation (ENSO) (Saji et al., 1999; Loschnigg et al., 2003; Stuecker et al., 2017), emphasizing the close relationship between the IOD and ENSO. When El Niño happens, the Walker circulation is weakened. Subsequently, the anomalous divergence in the Indo-Pacific warm pool further induces anomalous easterly winds near Sumatra. These easterly wind anomalies are favorable for upwelling in that region, and thus the appearance of a positive IOD event (Yu and Lau, 2005; Zhang et al., 2015). Therefore, ENSO is one important forcing that induces the appearance of IOD events (Li et al., 2003). Furthermore, ENSO also favors the appearance of the basin-wide

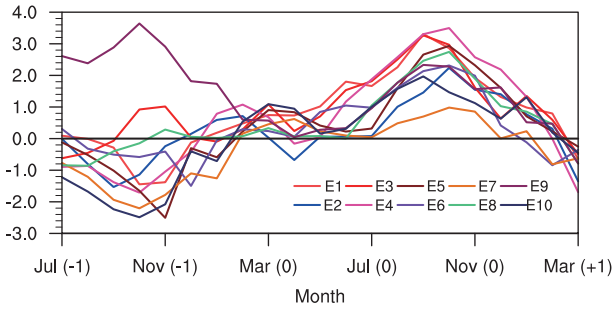

Fig. 1. Evolution of DMIs for 10 reference IOD events. E1–E10 signify the positive IOD events, with the model years 1, 3, 11, 20, 24, 59, 81, 88, 90, and 95, respectively. "−1" signifies the year preceding the IOD year; "0" signifies the IOD year; and "+" signifies the year following the IOD year.

wintertime surface warming in the tropical Indian Ocean under the combined effects of the anomalous latent heat flux and solar radiation, resulting in the decay of IOD events (Chowdary and Gnanaseelan, 2007). In short, ENSO affects not only the occurrence, but also the development, of IOD events. The role of ENSO should not be ignored when exploring the predictability of IOD events.

It has been previously shown that a WPB and an SPB exist in IOD predictions, which are respectively related to the initial errors in the tropical Indian and Pacific oceans (Feng et al., 2014a; Liu et al., 2018). In this study, we found that, in addition to the WPB, the initial errors in the tropical Indian Ocean also yield a significant SPB, which greatly affects the summertime predictions of IOD events. That is, not only the initial errors in the tropical Pacific Ocean, but also those in the tropical Indian Ocean could yield a significant SPB. Based on the above context, in this paper, we mainly discuss the role of initial errors in the tropical Indian Ocean, as well as the role of ENSO, on IOD predictions. In particular, the discussion will primarily focus on the SPB phenomenon. Due to the increasing frequency of occurrence under global warming and the larger climatic effects for positive IOD events compared with negative ones (Vinayachandran et al., 2002; Black et al., 2003; Annamalai and Murtugudde, 2004; Behera et al., 2005; Cai et al., 2009; Weller and Cai, 2013), the focus is restricted to positive events.

The remainder of the paper is organized as follows: The model and the experimental strategy are described in section 2. The predictability barriers caused by initial errors, as well as the influence upon them from ENSO, are analyzed in section 3. The spatial pattern of predictability barrier–related initial errors and their developmental physical mechanisms are explored in section 4. Finally, a summary and discussion is provided in section 5.

2. Model and experimental strategy

The Geophysical Fluid Dynamics Laboratory Climate Model, version 2p1 (GFDL CM2p1), an ocean–atmosphere–land–ice coupled model, is used to explore the effects of initial errors in the tropical Indian Ocean on IOD predictions. The oceanic component is the Modular Ocean Model, version 4 (Griffies, 2009), with a horizontal resolution of $1^\circ \times 1^\circ$ in most regions, and a meridional resolution reducing to $1/3^\circ$ near the equator. In the vertical direction, there are a total of 50 levels, and the resolution varies with depth, with a 10-m resolution in the upper 225 m. The atmospheric component of the coupled model is the GFDL atmosphere model, AM2p12b (GFDL Global Atmospheric Model Development Team, 2004). Its horizontal resolution is 2.5° longitude by 2° latitude, with 24 levels in the vertical direction. The different components couple with each other via the GFDL's Flexible Modeling System (http://www.gfdl.noaa.gov/fms). Feng et al. (2014b) evaluated 14 models within phase 5 of the Coupled Model Intercomparison Project and demonstrated that GFDL CM2p1 is one of four models that can capture the cli-

matology in the tropical Indian Ocean and the basic characteristics of IOD events. Therefore, it is reasonable to study the predictability of IOD events using GFDL CM2p1.

The GFDL CM2p1 coupled model is run for 150 years under the forcings of land cover, insolation, aerosols and tracer gases in 1990. Only the last 100 years are studied, to exclude the effects of the initial adjustment process in the first 50 years. Ten positive IOD events, i.e., where the DMI exceeds 0.5 for at least three consecutive months (Song et al., 2007), are randomly selected from the 100-year integration as the "true states", i.e., reference states, to be predicted. The DMIs of these IOD events generally reverse the sign in winter, develop in summer, peak in autumn, and decay rapidly in the following winter (Fig. 1), which is consistent with observational results (Wajsowicz, 2004).

Perfect model predictability experiments are conducted in this study. That is, the model is assumed to be perfect, and the prediction errors are only caused by the initial errors. As the ocean actively forces the atmosphere in the tropical oceans in most cases, the sea temperature only is perturbed to explore the effects of initial errors on IOD predictions. However, perturbing all levels of see temperature in the tropical Indian Ocean will cause incompatibility between the initial fields and the model, which further results in robust initial shock and conceals the effects of initial errors on IOD predictions, especially in the first few months. Therefore, we step back and only superimpose the initial errors on several important levels of sea temperature. The thermocline depth in the tropical Indian Ocean, which is closely related to the development of IOD events, is about 100–130 m in GFDL CM2p1 (Song et al., 2007). Therefore, the perturbations on the sea temperature at the depth of 95 m, which is close to the thermocline depth, would quickly affect the surrounding sea temperature and may reflect the variation of thermocline depth to some extent. Meanwhile, the sea surface temperature (SST) connects the atmosphere and the ocean, and is also closely related to the evolution of IOD events. Therefore, initial sea temperature errors are only superimposed on two levels of sea temperatures, i.e., the temperatures at the sea surface and at the depth of 95 m.

It is demonstrated that initial errors that cause large prediction uncertainties for ocean–atmosphere coupled phenomena, such as ENSO and the Kuroshio Large Meander, usually have a dynamic developmental behavior similar to these events themselves (Yu et al., 2009; Wang et al., 2012; Duan et al., 2013). Therefore, to explore the predictability barriers caused by the initial errors in the tropical Indian Ocean, we generate the initial errors from IOD-related sea temperature anomalies. Furthermore, the period of IOD events in GFDL CM2p1 is four years (Feng et al., 2014a). That is, there is generally a positive and a negative IOD event within four years. Hence, the sea temperature anomalies in the four years preceding each positive IOD event are plentiful and sampled every other month to generate lentiful initial errors. That is, there are 24 pairs of initial errors for each reference IOD event.

To impartially compare the effects of different initial errors on IOD predictions, all the initial errors are scaled to the same magnitude and then superimposed on the initial field of the reference-state IOD events. The original SSTAs and temperatures at 95 m deep are signified as T_1 and T_2, which are scaled by $T_1' = T_1/\delta_1$ and $T_2' = T_2/\delta_2$, respectively, where δ_1 and δ_2 signify positive values. T_1' and T_2' denote the surface and subsurface components of the scaled initial errors superimposed on the initial fields, respectively. The norms of the scaled initial errors, $\|T_1'\| = \sqrt{\sum_{i,j}(T'_{1,i,j})^2}$ and $\|T_2'\| = \sqrt{\sum_{i,j}(T'_{2,i,j})^2}$, are set as 2.4°C, where the grid point (i, j) covers the tropical Indian Ocean, i.e., (10°S–10°N, 45°–115°E). It is shown in Kaplan et al. (1998) that the standard deviation of analysis errors for sea temperature near the equator is about 0.2°C, which is larger than the initial errors generated in this study in each grid. Therefore, these initial errors probably exist in analysis errors and the magnitude of our initial errors is reasonable. The spatial patterns of two samples of initial errors are shown in Fig. 2, as well as the spatial pattern of the initial field of one reference-state IOD event.

After superimposing the initial errors on the initial field of the reference-state IOD events, the predictions are started from July and October in the year preceding the IOD year with a lead time of 12 months. For simplicity, in the following discussions, the start months are signified as July(−1) and October(−1), respectively, where (−1) signifies the year preceding the IOD year. Therefore, we obtain 240 predictions for each start month. The prediction errors are then calculated as the absolute values of the difference in the DMI between the predicted IOD events and the "true state" of IOD events. As perfect model predictability experiments are carried out in this study, the prediction errors here are only caused by the initial errors. The growth rates of prediction errors η are calculated as

$$\eta = \frac{\partial E(t)}{\partial t} \approx \frac{E(t_2) - E(t_1)}{t_2 - t_1},$$

where $E(t_1)$ and $E(t_2)$ denote the prediction errors at times t_1 and t_2, respectively. The difference between t_2 and t_1 is one month in this study, which indicates that η signifies the monthly growth rates of prediction errors. A positive (negative) value of η indicates that the prediction errors increase (decrease). The larger the positive value of η, the faster the increase in the prediction errors.

3. Predictability barriers induced by initial errors in the tropical Indian Ocean

In this section, by analyzing the growth rates of prediction errors in 240 predictions for each start month, predictability barriers are identified, as well as their relationship with ENSO. We divided each calendar year into four "seasons", with December–February as boreal winter, March–May as boreal spring, and so on. As the results are similar between the start months of July(−1) and October(−1), only those for the start month of July(−1) are shown in the following dis-

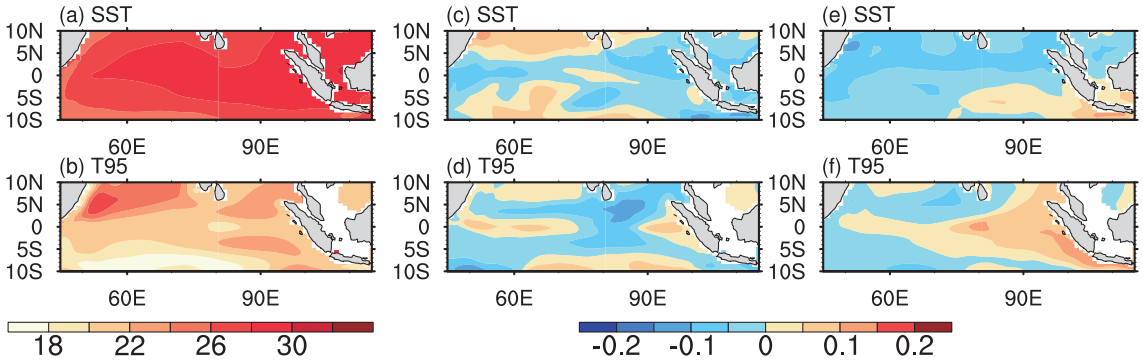

Fig. 2. Spatial pattern of the initial field of a given reference-state IOD event at (a) the sea surface and (b) 95 m deep, in the tropical Indian Ocean (left-hand column; units: °C). The middle and right-hand columns denote the spatial patterns of two samples of initial errors at (c, e) the sea surface and (d, f) 95 m deep, respectively.

cussions.

Table 1 shows the existence of ENSO in the different developmental phases of 10 positive IOD events. In the winter of the growing phase, four IOD events are accompanied by a decaying El Niño or La Niña, with the remaining IOD events being independent of ENSO. In spring and summer, seven IOD events are accompanied by a developing El Niño or La Niña, with the remaining IOD events unassociated with ENSO. Therefore, the relationship between the IOD and ENSO varies in different developmental phases of IOD events. It is thus necessary to separately explore the effects of ENSO on IOD predictions according to the different developmental phases of IOD events.

Figure 3 shows the monthly growth rates of prediction errors for each reference IOD event based on 24 predictions. It is evident that the prediction errors develop rapidly in two main periods, i.e., the winter and the late spring/early summer in the growing phase of IOD events. Specifically, when the monthly growth rate is the largest or the second largest in winter (in late spring/early summer, i.e., in May), and the value of the monthly growth rate is larger than 0.2, a significant WPB (SPB) phenomenon occurs in IOD predictions. It is found that a significant WPB phenomenon exists in predictions of six reference IOD events. These reference IOD events, coincidentally, are independent of ENSO in the winter of the growing phase. In contrast, no WPB occurs in the predictions of the other four reference IOD events, which are accompanied by ENSO in winter. That is, when ENSO exists in the winter of the growing phase, it is not favorable for the occurrence of the WPB. A previous study demonstrated that ENSO favors the appearance of a basin-wide surface warming in winter under the combined effects of ocean dynamics, latent heat flux and solar radiation (Chowdary and Gnanaseelan, 2007). Here, it is found that ENSO also affects the development of temperature errors and favors a basin-wide mode of temperature errors in the tropical Indian Ocean in the winter of the growing phase (figure omitted), which might be based on a similar physical mechanism. This results in small prediction errors in winter, and thus no appearance of the WPB. In addition to the WPB, a significant SPB phenomenon exists in six reference IOD events, regardless of whether these IOD events are accompanied by ENSO in spring and summer. That is, there is no inherent connection between the occurrence of the SPB and ENSO. Based on the above discussions, the existence of ENSO is only closely connected with the occurrence of the WPB in IOD predictions.

Table 1. Existence of ENSO (El Niño/La Niña) in different seasons in the growing phase of IOD events. The first column denotes ten reference-state IOD years in the model. The words "El Niño" and "La Niña" indicate that the IOD events are accompanied by El Niño or La Niña; the symbol "—" signifies that there is only IOD events.

Reference IOD events	Winter	Spring and summer
1	La Niña	—
3	—	El Niño
11	—	—
20	—	El Niño
24	—	El Niño
59	La Niña	—
81	—	El Niño
88	—	El Niño
90	El Niño	La Niña
95	La Niña	El Niño

The largest monthly growth rate of prediction errors in each prediction is labeled as $\eta_{\max}$ and the second largest as $\eta_{s\text{-}\max}$. If $\eta_{\max}$ occurs in winter and the difference between $\eta_{\max}$ and $\eta_{s\text{-}\max}$ is larger than 0.3, the corresponding initial errors are selected as those that are most likely to yield a significant WPB and defined as WPB-related initial errors. SPB-related initial errors are similarly selected. In total, there are 39 WPB-related initial errors and 31 SPB-related initial errors. The DMI errors (i.e., the difference in the DMI between the predictions and the corresponding reference IOD event) for these initial errors are shown in Fig. 4. The DMI errors for WPB-related initial errors are large (positive or negative) in winter, which results in large prediction uncertainties and causes the low forecast skill of IOD occurrence. For SPB-related initial errors, there are large negative DMI errors in summer, indicating that positive IOD events are generally predicted as weaker positive events, or even as negative events, causing the low forecast skill of IOD intensity.

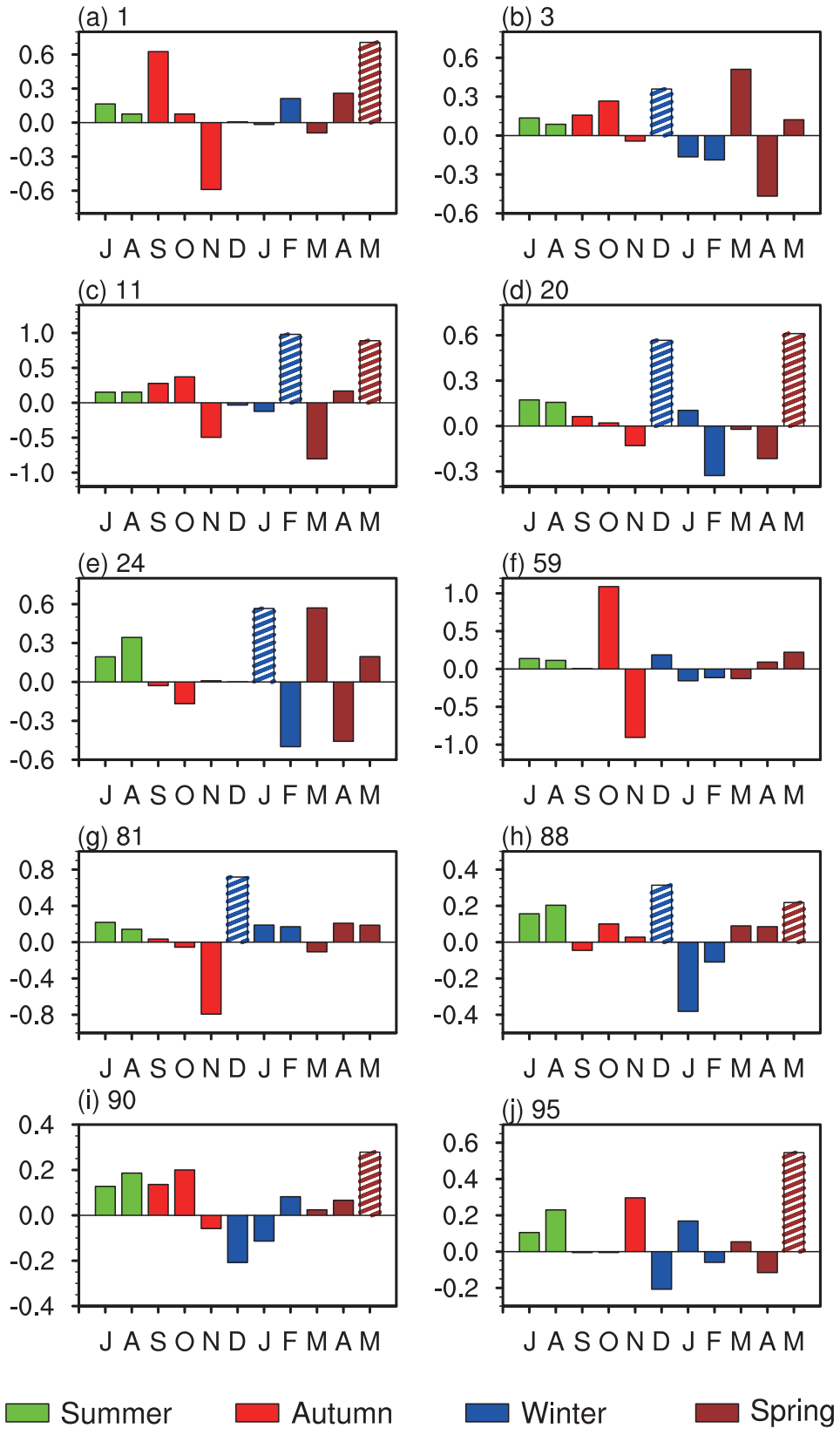

Fig. 3. Monthly growth rates of prediction errors for 10 reference IOD events (units: month^{-1}). Panels (a–j) denote 10 reference IOD events with the model years 1, 3, 11, 20, 24, 59, 81, 88, 90, and 95, respectively. Each letter on the horizontal axes denotes the first letter of different months. The vertical axes denote the growth rates of prediction errors. The four colors indicate the four seasons. The blue and brown bars with diagonal stripes correspond to the WPB and SPB in IOD predictions, respectively.

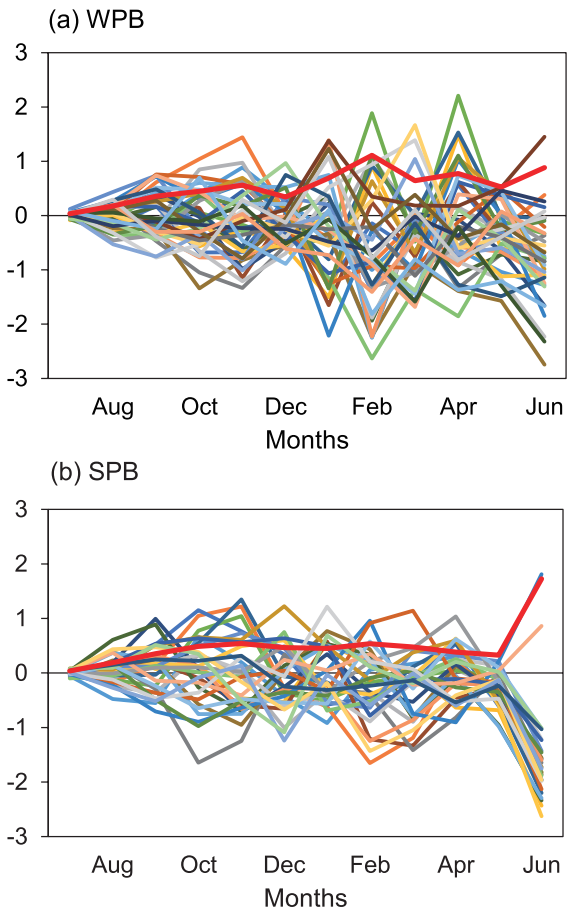

Fig. 4. Time-dependent evolutions of DMI errors for initial errors that yield a significant (a) WPB and (b) SPB. Red lines denote the ensemble mean of prediction errors for WPB- and SPB- related initial errors, respectively. Each of the other colored lines denotes an individual prediction.

Besides, the mean absolute value of the DMI errors (i.e., mean prediction error) for SPB-related initial errors in summer is larger than that for WPB-related initial errors in winter, indicating larger prediction uncertainties in summer.

4. Spatial patterns of predictability barrier–related initial errors and their developmental physical mechanisms

In this section, we explore the dominant spatial patterns of initial errors that are most likely to yield significant predictability barriers, and analyze their developmental physical mechanisms. As WPB-related initial errors have already been discussed in Feng et al. (2017), we briefly analyze SPB-related initial errors in this study.

4.1. *Spatial patterns of initial errors that induce a significant SPB*

As stated above, 31 SPB-related initial errors were selected in section 3. We put these initial errors together and assume them as time-varying fields corresponding to 31 different time points. Then, empirical orthogonal function (EOF) analysis is applied to these initial errors and the leading EOF mode (i.e., EOF1) is obtained, which describes the dominant spatial patterns of SPB-related initial errors. Corresponding to the EOF1 mode, the time series (i.e., PC1) has positive and negative values, indicating that some SPB-related initial errors have similar spatial patterns to the EOF1 mode and others have opposite ones. Therefore, the SPB-related initial errors are classified into two categories. The SPB-related initial errors that correspond to positive values of PC1 comprise the first category, and their composite is defined as type-1 initial error. Similarly, the composite of the SPB-related initial errors corresponding to the negative values of PC1 is defined as type-2 initial error.

Type-1 initial error shows a significant west–east dipole pattern, both in the surface and subsurface components, with negative values in the western Indian Ocean and positive values in the eastern Indian Ocean (Fig. 5). The largest absolute values of type-1 initial error are concentrated in the subsurface component of the eastern tropical Indian Ocean. Type-2 initial error is almost opposite to type-1 initial error. Interestingly, the dominant spatial patterns of SPB-related initial errors in the tropical Indian Ocean are similar to those of the WPB-related initial errors analyzed in Feng et al. (2017). The absolute values of spatial correlation coefficients between them are larger than 0.89. Therefore, initial errors with a west–east dipole pattern in the tropical Indian Ocean are inclined to yield a significant WPB and SPB, which results in large prediction uncertainties in winter and summer, and greatly limits the forecasting skill of the occurrence and the intensity of IOD events. Feng et al. (2017) demonstrated that the subsurface eastern tropical Indian Ocean is the potential observing location (i.e., sensitive area) for advancing beyond the WPB for positive IOD events. That is, if intensive observations are carried out over this area, it will reduce the prediction errors in winter and weaken the WPB, improving the skill of wintertime IOD-event forecasts. Notably, the large values of SPB-related initial errors are also concentrated in the subsurface eastern Indian Ocean. That is, the initial errors in this area contribute greatly to the prediction uncertainties of positive IOD events. Therefore, if intensive observations are carried out over this area, it will not only weaken the WPB, but also reduce the prediction uncertainties in summer, and further weaken the SPB, ultimately greatly improving the forecasting skill with respect to the occurrence and intensity of positive IOD events.

Based on the above discussions, in addition to the initial errors in the tropical Pacific Ocean (Liu et al., 2018), the initial errors in the tropical Indian Ocean also play an important role in yielding a significant SPB. Therefore, to reduce the prediction uncertainties in summer and weaken the SPB, initial errors in the Indian Ocean should also be considered.

4.2. *Developmental physical mechanisms of initial errors that induce a significant SPB*

In this section, we calculate the sea temperature anomalies, which are defined as the difference in the sea temperature

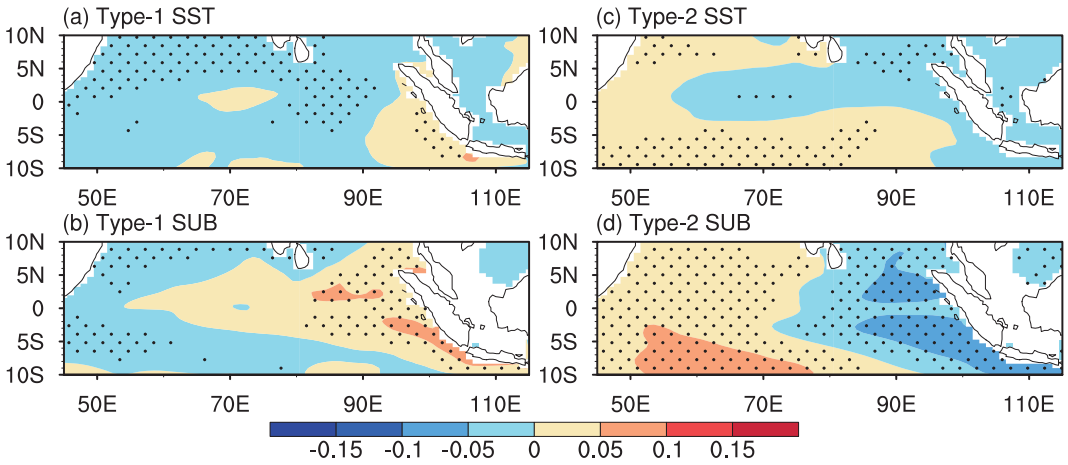

Fig. 5. Spatial patterns of two types of SPB-related initial errors (units: °C). Panels (a, b) denote the surface and subsurface components for type-1 initial error; panels (c, d) denote the surface and subsurface components for type-2 initial error. Dotted areas indicate that the composites of temperature errors exceed the 95% confidence level, as determined by the *t*-test.

between the predictions and the "true state" of IOD events. Similarly, surface wind anomalies are also defined and calculated. Then, by analyzing the evolution of these temperature and wind anomalies, we identify how the SPB-related initial errors develop and cause large prediction uncertainties in summer, ultimately resulting in a significant SPB. Although type-1 and type-2 initial errors have opposite spatial patterns, the dominant characteristics of their evolution are only different in the first month and almost the same in the rest of the prediction year. Therefore, the evolution of the temperature and wind anomalies for two types of SPB-related initial errors is shown together in Fig. 6.

When SPB-related initial errors are superimposed on the initial field of the reference-state IOD events, significant SST anomalies appear in the tropical Pacific Ocean in August, with positive values in the western Pacific Ocean and negative values in the central-eastern Pacific Ocean (Fig. 6). In the meantime, significant temperature anomalies appear in the subsurface Indian Ocean, with negative values in the western Indian Ocean and positive values in the eastern Indian Ocean. It is noted that the SST anomalies in the tropical Indian Ocean are relatively small in August and September. Therefore, the westerly wind anomalies at the equator in the tropical Indian Ocean may not be due to the local SST anomalies, but induced by the SST anomalies in the tropical Pacific Ocean. Specifically, the zonal SST gradient in the tropical Pacific Ocean causes easterly wind anomalies at the equator, which further modulate the Walker circulation in tropical oceans and induce anomalous westerly wind in the tropical Indian Ocean (Chen, 2011; Lian et al., 2014). Then, the anomalous westerly wind piles up warm water in the eastern Indian Ocean, and strengthens the subsurface warming there.

In the first half of the prediction year, the positive temperature anomalies in the subsurface eastern Indian Ocean indicate a deepening of the thermocline depth and an increase in the sea surface height (SSH). This will reduce the translation of the warm water from the western Pacific Ocean to the eastern Indian Ocean, resulting in the deepening of the thermocline depth and the warming of the subsurface ocean in the western Pacific Ocean. The positive subsurface temperature anomalies further propagate eastward to the eastern Pacific Ocean, and cause the warming of the ocean and the weakening of the negative SST anomalies there. In January–March, in response to the zonal gradient of the surface temperature anomalies in the tropical Pacific Ocean, westerly wind anomalies appear at the equator in the central-eastern Pacific Ocean, which further induce easterly wind anomalies in the tropical Indian Ocean by modulating the Walker circulation in tropical oceans. On the one hand, the anomalous easterly wind favors upwelling to the coast of Sumatra and Java, resulting in an elevation of the thermocline depth and a decrease in the SSH, which advances the translation of the warm water from the western Pacific Ocean into the eastern Indian Ocean. This further results in an elevation of the thermocline depth and negative subsurface temperature anomalies in the western Pacific Ocean, which propagate eastward to the eastern Pacific Ocean to cool the ocean there. On the other hand, the southeast wind anomalies in the eastern Indian Ocean are opposite in direction to the climatological wind, which decreases the total wind speed, and thus the release of the latent heat flux from ocean to atmosphere, warming the sea surface water there. With the eastward propagation of the negative temperature anomalies in the Pacific Ocean and the warming of the sea surface water in the eastern Indian Ocean, northwest wind anomalies appear in the Indian Ocean in April–June. In summer, the northwest wind anomalies are opposite in direction to the climatological wind in the eastern Indian Ocean, which decreases the total wind speed and thus the release of latent heat flux from ocean to atmosphere, finally warming the sea surface water. Therefore, a significant west–east dipole pattern of SST anomalies appears, which is further strengthened under the effect of

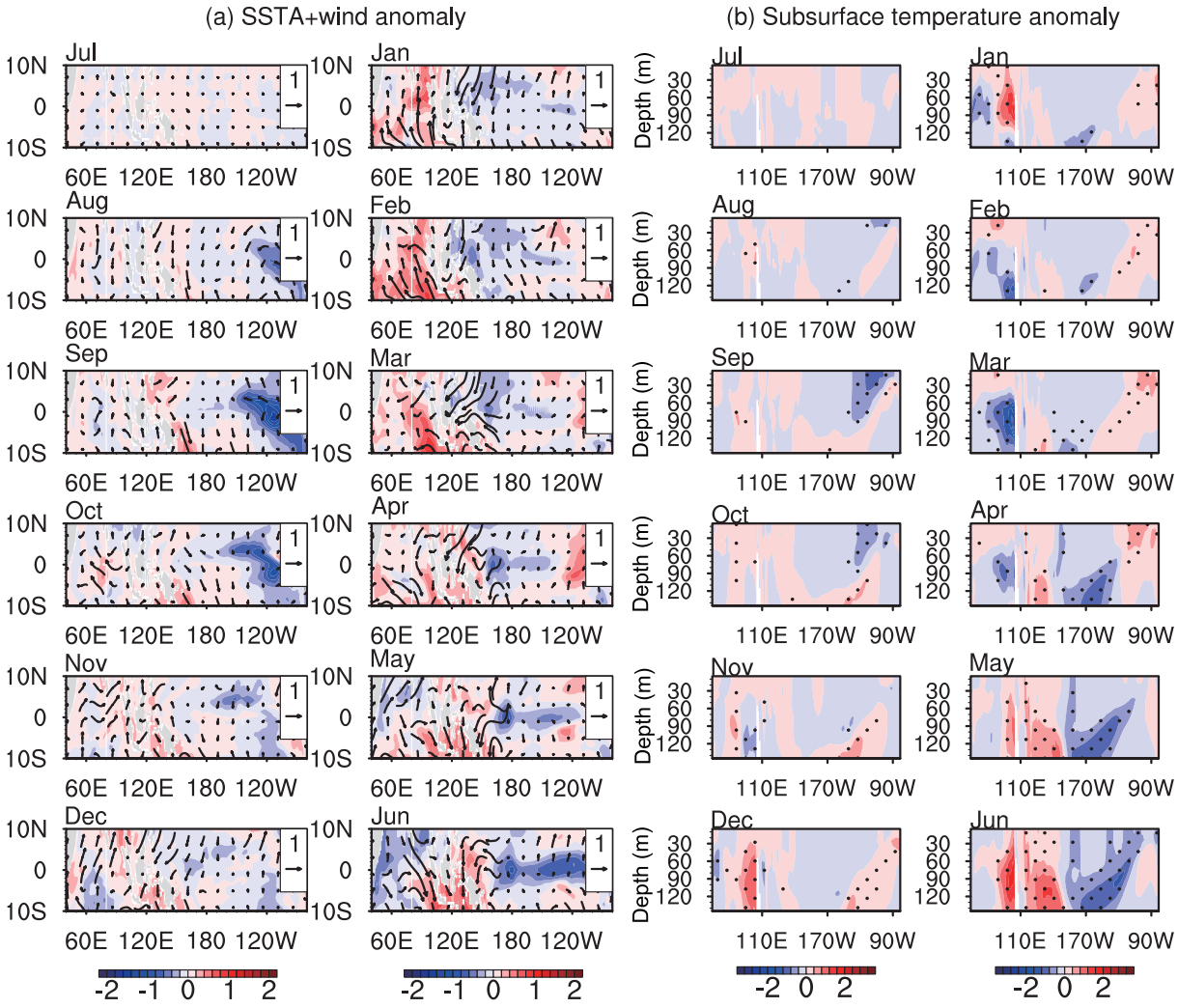

Fig. 6. Evolutions of the SSTA (units: °C) and sea surface wind anomaly (units: m s^{-1}) over the tropical Indian and Pacific oceans (left-hand column), and the equatorial (5°S–5°N) subsurface temperature anomaly (units: °C; right-hand column) for SPB-related initial errors. Dotted areas indicate that the composites of temperature anomalies exceed the 95% confidence level, as determined by the *t*-test.

Bjerknes feedback, ultimately resulting in a significant SPB.

Furthermore, we also analyze the evolution of sea temperature and surface wind anomalies for one sample of initial error that does not yield a significant SPB (Fig. 7). It is found that the SST anomalies grow fast and present a significant west–east dipole pattern in winter, which indicates large prediction errors in winter. In contrast, the SST anomalies show a basin-wide warming in summer, indicating small prediction errors in summer and thus no occurrence of an SPB.

Based on the above discussions, although initial errors are superimposed on the tropical Indian Ocean only, they further cause temperature and wind anomalies in the tropical Pacific Ocean. The interaction between the Indian and Pacific oceans plays an important role in yielding a significant SPB. That is, if there is no Pacific Ocean, and only the Indian Ocean exists in models, no SPB is likely to occur in IOD predictions, even though dipole-pattern initial errors exist in the tropical Indian Ocean. Therefore, the Pacific Ocean is indispensable in yielding a significant SPB.

5. Summary and discussion

Using the GFDL CM2p1 coupled model, the role of initial errors in the tropical Indian Ocean is explored in this paper by conducting perfect-model predictability experiments. Furthermore, the effects of ENSO on IOD predictability are also identified.

The WPB exists in predictions of six reference IOD events, which are independent of ENSO in the winter of the growing phase. In contrast, no WPB occurs in the predictions of the remaining reference IOD events accompanied by ENSO in winter. That is, ENSO in the winter of the growing phase is not favorable for the occurrence of the WPB. Therefore, the existence of ENSO in winter generally causes small prediction errors in winter, and is thus favorable for skillful forecasting of IOD occurrence. In addition to the WPB, an

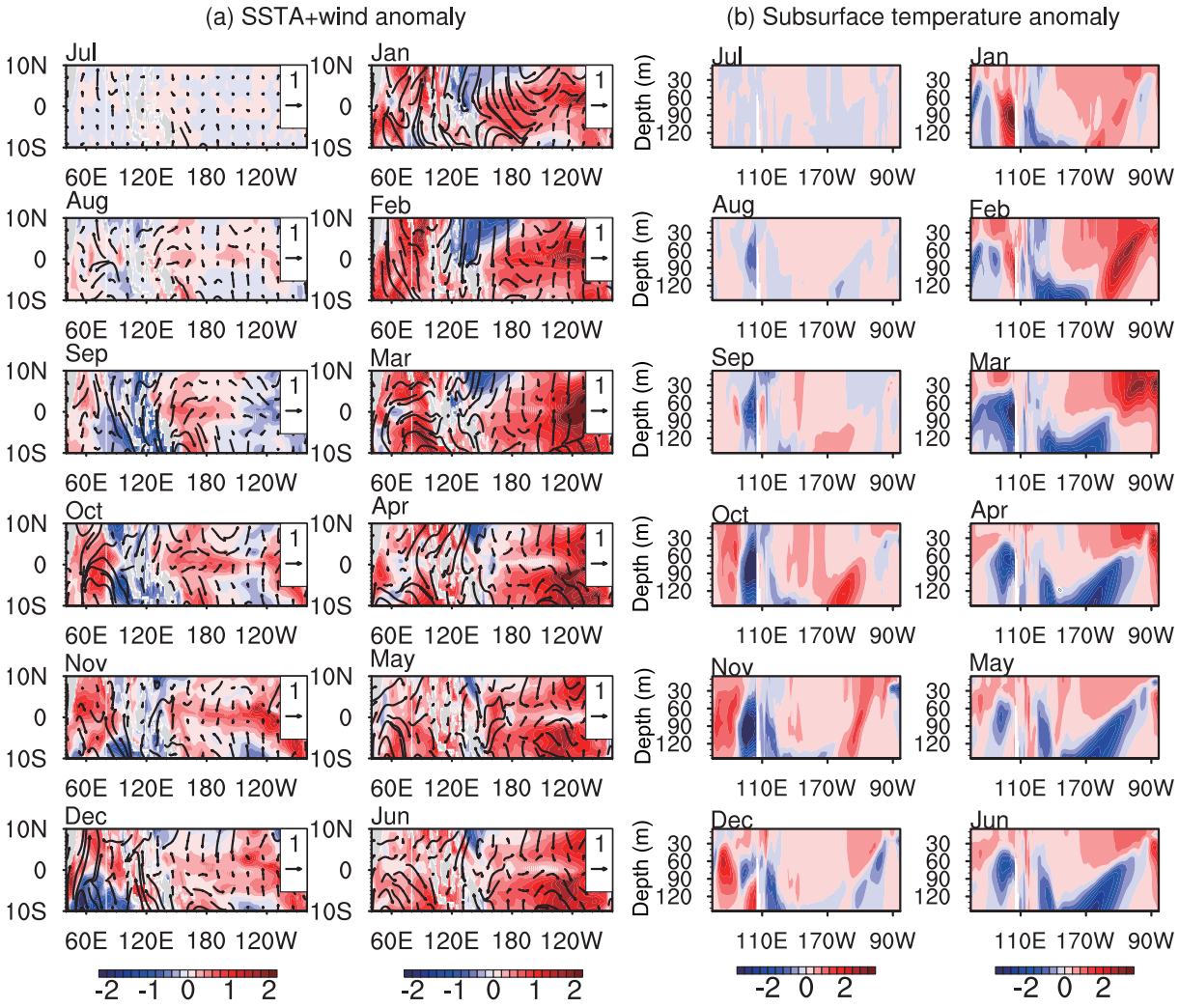

Fig. 7. As in Fig. 6 but for one sample of initial error that does not yield a SPB.

SPB also exists in IOD predictions, which has no direct interaction with ENSO.

There are two types of SPB-related initial errors. Type-1 initial error presents a west–east dipole pattern in both the surface and subsurface components, with the largest absolute values of errors concentrated in the subsurface eastern Indian Ocean. Type-2 initial error shows an opposite spatial pattern to type-1 error. The dominant spatial patterns of SPB-related initial errors are similar to those of WPB-related initial errors, with the largest absolute values concentrated within the same area. It was demonstrated in Feng et al. (2017) that the subsurface eastern Indian Ocean is a sensitive area for advancing beyond the WPB. Therefore, if intensive observations are carried out in this area, not only will the WPB be weakened, but the prediction uncertainties in summer will also be reduced and the SPB weakened, greatly improving the forecasting skill of the occurrence and intensity of positive IOD events.

When SPB-related initial errors are superimposed on the initial field of the reference IOD events, significant SST anomalies appear in the tropical Pacific Ocean. By modulating the Walker circulation, anomalous westerly wind is induced in the tropical Indian Ocean, which piles up warm water in the eastern Indian Ocean, and thus causes a deepening of the thermocline depth and an elevation of the SSH in the eastern Indian Ocean. This further reduces the translation of the warm water from the western Pacific Ocean to the eastern Indian Ocean, resulting in the deepening of the thermocline depth and positive subsurface temperature anomalies in the western Pacific Ocean. The positive temperature anomalies propagate eastward to the eastern Pacific Ocean and warm the ocean there. Similarly, in the second half of the prediction year, the anomalous easterly wind appears in the tropical Indian Ocean, which causes upwelling and elevation of the thermocline depth in the eastern Indian Ocean and induces negative temperature anomalies in the western Pacific Ocean. The negative temperature anomalies propagate eastward and cool the sea water in the eastern Pacific Ocean. Furthermore, the anomalous easterly wind features wind of opposite direction to the climatology in the eastern Indian Ocean, which reduces the total wind speed and thus the release of latent heat flux from ocean to atmosphere, ultimately warming the sea

water in the eastern Indian Ocean. In response to these SST anomalies, westerly wind anomalies appear in the tropical Indian Ocean and are opposite in direction to the climatological wind in summer, which warms the sea surface water in the eastern Indian Ocean by decreasing the release of latent heat flux from ocean to atmosphere, finally forming a significant west–east dipole pattern and thus a significant SPB.

Liu et al. (2018) demonstrated that initial errors in the tropical Pacific Ocean are favorable for the occurrence of the SPB and identified its important role in yielding a significant SPB. Here, we find that, in addition to the initial errors in the tropical Pacific Ocean, those in the tropical Indian Ocean are also non-negligible. Of note is that, although the initial errors are superimposed on the tropical Indian Ocean only in this study, these initial errors further advance the occurrence of the SPB by modulating the temperature and wind anomalies in the tropical Pacific Ocean. Therefore, the role of the Pacific Ocean is indispensable in yielding an SPB.

Based on the above discussions, both the initial errors in the tropical Indian and Pacific oceans could induce a significant SPB. Therefore, to reduce the prediction uncertainties in summer and weaken the SPB, the initial errors in the Pacific and Indian oceans need to be reduced by carrying out intensive observations. Furthermore, due to the high degree of similarity in the spatial patterns between WPB-related initial errors and SPB-related initial errors in the tropical Indian Ocean, if intensive observations were to be carried out over the eastern subsurface Indian Ocean, this will not only reduce the prediction uncertainties in winter, but also in summer, thus weakening the WPB and SPB. Therefore, by increasing the intensity of observations in the tropical Indian and Pacific oceans, it will considerably reduce the prediction uncertainties and greatly improve the forecasting skill with respect to the occurrence and intensity of IOD events. Furthermore, Sayantani et al. (2014) demonstrated that the Arabian Sea plays an important role in the evolution of IOD. Therefore, in addition to the initial errors in the tropical oceans, those in the Arabian Sea might also affect the IOD predictability, which needs to be further investigated and discussed in a future study.

Acknowledgements. This work was jointly sponsored by the National Key Research and Development Program of China (Grant No. 2017YFA0604201), the Strategic Priority Research Program of Chinese Academy of Sciences (Grant No. XDA20060501), the National Natural Science Foundation of China (Grant Nos. 41876024 and 41530961), and the National Programme on Global Change and Air–Sea Interaction (Grant No. GASI-IPOVAI-06).

REFERENCES

Annamalai, H., and R. Murtugudde, 2004: Role of the Indian Ocean in regional climate variability. *Earth's Climate*: *The Ocean-Atmosphere Interaction*, C. Wang et al., Eds., American Geophysical Union, 213–246.

Ansell, T., C. J. C. Reason, and G. Meyers, 2000: Variability in the tropical southeast Indian Ocean and links with southeast Australian winter rainfall. *Geophys. Res. Lett.*, **27**, 3977–3980, https://doi.org/10.1029/2000GL011856.

Behera, S. K., J. J. Luo, S. Masson, P. Delecluse, S. Gualdi, A. Navarra, and T. Yamagata, 2005: Paramount impact of the Indian Ocean dipole on the East African short rains: A CGCM study. *J. Climate*, **18**, 4514–4530, https://doi.org/10.1175/JCLI3541.1.

Black, E., J. Slingo, and K. P. Sperber, 2003: An observational study of the relationship between excessively strong short rains in coastal east Africa and Indian Ocean SST. *Mon. Wea. Rev.*, **131**(1), 74–94, https://doi.org/10.1175/1520-0493(2003)131<0074:AOSOTR>2.0.CO;2.

Cai, W., T. Cowan, and A. Sullivan, 2009: Recent unprecedented skewness towards positive Indian Ocean Dipole occurrences and its impact on Australian rainfall. *Geophys. Res. Lett.*, **36**, L11705, https://doi.org/10.1029/2009GL037604.

Cai, W. J., H. H. Hendon, and G. Meyers, 2005: Indian Ocean dipolelike variability in the CSIRO Mark 3 coupled climate model. *J. Climate*, **18**, 1449–1468, https://doi.org/10.1175/JCLI3332.1.

Chen, D. K., 2011: Indo-Pacific tripole: An intrinsic mode of tropical climate variability. *Advances in Geosciences*, **24**, 1–18.

Chowdary, J. S., and C. Gnanaseelan, 2007: Basin-wide warming of the Indian Ocean during El Niño and Indian Ocean dipole years. *International Journal of Climatology*, **27**, 1421–1438, https://doi.org/10.1002/joc.1482.

Duan, W. S., Y. S. Yu, H. Xu, and P. Zhao, 2013: Behaviors of nonlinearities modulating the El Niñno events induced by optimal precursory disturbances. *Climate Dyn.*, **40**, 1399–1413, https://doi.org/10.1007/s00382-012-1557-z.

Feng, R., and W. S. Duan, 2018: Investigating the initial errors that cause predictability barriers for Indian Ocean Dipole events using CMIP5 model outputs. *Adv. Atmos. Sci.*, **35**(10), 1305–1320, https://doi.org/10.1007/s00376-018-7214-7.

Feng, R., W. S. Duan, and M. Mu, 2014a: The "winter predictability barrier" for IOD events and its error growth dynamics: Results from a fully coupled GCM. *J. Geophys. Res.*, **119**, 8688–8708, https://doi.org/10.1002/2014JC010473.

Feng, R., M. Mu, and W. S. Duan, 2014b: Study on the "winter persistence barrier" of Indian Ocean dipole events using observation data and CMIP5 model outputs. *Theor. Appl. Climatol.*, **118**(3), 523–534, https://doi.org/10.1007/s00704-013-1083-x.

Feng, R., W. S. Duan, and M. Mu, 2017: Estimating observing locations for advancing beyond the winter predictability barrier of Indian Ocean dipole event predictions. *Climate Dyn.*, **48**, 1173–1185, https://doi.org/10.1007/s00382-016-3134-3.

GFDL Global Atmospheric Model Development Team, 2004: The new GFDL global atmosphere and land model AM2-LM2: Evaluation with prescribed SST simulations. *J. Climate*, **17**, 4641–4673, https://doi.org/10.1175/JCLI-3223.1.

Griffies, S. M., 2009: Elements of MOM4p1: GFDL ocean group. Technical Report No.6, 444 pp.

Gualdi, S., E. Guilyardi, A. Navarra, S. Masina, and P. Delecluse, 2003: The interannual variability in the tropical Indian Ocean as simulated by a CGCM. *Climate Dyn.*, **20**, 567–582, https://doi.org/10.1007/s00382-002-0295-z.

Kaplan, A., M. A. Cane, Y. Kushnir, A. C. Clement, M. B. Blumenthal, and B. Rajagopalan, 1998: Analyses of global sea surface temperature 1856-1991. *J. Geophys. Res.*, **103**, 18 567–185 89, https://doi.org/10.1029/97JC01736.

Li, T., B. Wang, C. P. Chang, and Y. S. Zhang, 2003: A

theory for the Indian Ocean dipole-zonal mode. *J. Atmos. Sci*., **60**(17), 2119–2135, https://doi.org/10.1175/1520-0469(2003)060<2119:ATFTIO>2.0.CO;2.

Lian, T., D. K. Chen, Y. M. Tang, and B. G. Jin, 2014: A theoretical investigation of the tropical Indo-Pacific tripole mode. *Science China Earth Sciences*, **57**, 174–188, https://doi.org/10.1007/s11430-013-4762-7.

Liu, D., W. S. Duan, R. Feng, and Y. M. Tang, 2018: Summer Predictability Barrier of Indian Ocean dipole events and corresponding error growth dynamics. *J. Geophys. Res*., **123**, 3635–3650, https://doi.org/10.1029/2017JC013739.

Loschnigg, J., G. A. Meehl, P. J. Webster, J. M. Arblaster, and G. P. Compo, 2003: The Asian monsoon, the tropospheric biennial oscillation, and the Indian Ocean zonal mode in the NCAR CSM. *J. Climate*, **16**, 1617–1642, https://doi.org/10.1175/1520-0442(2003)016<1617:TAMTTB>2.0.CO;2.

Luo, J. J., S. Masson, S. Behera, S. Shingu, and T. Yamagata, 2005: Seasonal climate predictability in a coupled OAGCM using a different approach for ensemble forecasts. *J. Climate*, **18**(21), 4474–4497, https://doi.org/10.1175/JCLI3526.1.

Luo, J. J., S. Masson, S. Behera, and T. Yamagata, 2007: Experimental forecasts of the Indian Ocean dipole using a coupled OAGCM. *J. Climate*, **20**(10), 2178–2190, https://doi.org/10.1175/JCLI4132.1.

Murtugudde, R., J. P. McCreary Jr., and A. J. Busalacchi, 2000: Oceanic processes associated with anomalous events in the Indian Ocean with relevance to 1997–1998. *J. Geophys. Res*., **105**(C2), 3295–3306, https://doi.org/10.1029/1999JC900294.

Saji, N. H., and T. Yamagata, 2003: Possible impacts of Indian Ocean Dipole mode events on global climate. *Climate Research*, **25**, 151–169, https://doi.org/10.3354/cr025151.

Saji, N. H., B. N. Goswami, P. N. Vinayachandran, and T. Yamagata, 1999: A dipole mode in the tropical Indian Ocean. *Nature*, **401**(6751), 360–363, https://doi.org/10.1038/43854.

Sayantani, O., C. Gnanaseelan, and J. S. Chowdary, 2014: The role of Arabian Sea in the evolution of Indian Ocean Dipole. *International Journal of Climatology*, **34**, 1845–1859, https://doi.org/10.1002/joc.3805.

Shi, L., H. H. Hendon, O. Alves, J. J. Luo, M. Balmaseda, and D. Anderson, 2012: How predictable is the Indian Ocean dipole? *Mon. Wea. Rev*., **140**(12), 3867–3884, https://doi.org/10.1175/MWR-D-12-00001.1.

Song, Q., G. A. Vecchi, and A. J. Rosati, 2007: Indian Ocean variability in the GFDL coupled climate model. *J. Climate*, **20**, 2895–2916, https://doi.org/10.1175/JCLI4159.1.

Stuecker, M. F., A. Timmermann, F. F. Jin, Y. Chikamoto, W. J. Zhang, A. T. Wittenberg, E. Widiasih, and S. Zhao, 2017: Revisiting ENSO/Indian Ocean Dipole phase relationships, *Geophys. Res. Lett*., **44**, 2481–2492, https://doi.org/10.1002/2016GL072308.

Vinayachandran, P. N., S. Iizuka, and T. Yamagata, 2002: Indian Ocean dipole mode events in an ocean general circulation model. *Deep Sea Research Part II*: *Topical Studies in Oceanography*, **49**(7–8), 1573–1596, https://doi.org/10.1016/S0967-0645(01)00157-6.

Wajsowicz, R. C., 2004: Climate variability over the tropical Indian Ocean sector in the NSIPP seasonal forecast system. *J. Climate*, **17**(24), 4783–4804, https://doi.org/10.1175/JCLI-3239.1.

Wajsowicz, R. C., 2005: Potential predictability of tropical Indian Ocean SST anomalies. *Geophys. Res. Lett*., **32**(24), L24702. https://doi.org/10.1029/2005GL024169.

Wang, Q., M. Mu, and H. A. Dijkstra, 2012: Application of the conditional nonlinear optimal perturbation method to the predictability study of the Kuroshio large meander. *Adv. Atmos. Sci*., **29**(1), 118–134, https://doi.org/10.1007/s00376-011-0199-0.

Webster, P. J., A. M. Moore, J. P. Loschnigg, and R. R. Leben, 1999: Coupled ocean-atmosphere dynamics in the Indian Ocean during 1997–98. *Nature*, **401**(6751), 356–360, https://doi.org/10.1038/43848.

Weller, E., and W. J. Cai, 2013: Asymmetry in the IOD and ENSO teleconnection in a CMIP5 model ensemble and its relevance to regional rainfall. *J. Climate*, **26**, 5139–5149, https://doi.org/10.1175/JCLI-D-12-00789.1.

Yamagata, T., S. K. Behera, J. J. Luo, S. Masson, M. R. Jury, and S. A. Rao, 2004: Coupled ocean-atmosphere variability in the tropical Indian Ocean. *Earth's Climate*: *The Ocean-Atmosphere Interaction*, C. Wang, Eds., American Geophysical Union, 189–212.

Yu, J. Y., and K. M. Lau, 2005: Contrasting Indian Ocean SST variability with and without ENSO influence: A coupled atmosphere-ocean GCM study. *Meteor. Atmos. Phys*., **90**(3–4), 179–191, https://doi.org/10.1007/s00703-004-0094-7.

Yu, Y. S., W. S. Duan, and M. Mu, 2009: Dynamics of nonlinear error growth and season-dependent predictability of El Niño events in the Zebiak-Cane model. *Quart. J. Roy. Meteor. Soc*., **135**, 2146–2160, https://doi.org/10.1002/qj.526.

Zhang, W. J., Y. L. Wang, F. F. Jin, M. F. Stuecker, and A. G. Turner, 2015: Impact of different El Niño types on the El Niño/IOD relationship. *Geophys. Res. Lett*., **42**(20), 8570–8576, https://doi.org/10.1002/2015GL065703.

Zubair, L., S. A. Rao, and T. Yamagata, 2003: Modulation of Sri Lankan Maharainfall by the Indian Ocean dipole. *Geophys. Res. Lett*., **30**(2), 1063, https://doi.org/10.1029/2002GL015639.